The Astrophysical Journal, 777:169 (12pp), 2013 November 10 doi:10.1088/0004-637X/777/2/169

ZIRCONIUM—HAFNIUM ISOTOPE EVIDENCE FROM METEORITES FOR THE DECOUPLED SYNTHESIS OF LIGHT AND HEAVY NEUTRON-RICH NUCLEI

W. Akram[1,2], M. Schönbächler[1,2], P. Sprung[3], and N. Vogel[2,4]
[1] School of Earth, Atmospheric and Environmental Sciences, The University of Manchester, Oxford Road, Manchester, M13 9PL, UK
[2] Institute for Geochemistry and Petrology, ETH, Clausiusstrasse 25, 8092 Zürich, Switzerland
[3] Institut für Planetologie, Universität Münster, Wilhelm-Klemm-Strasse 10, D-48149 Münster, Germany
[4] Eawag, Swiss Federal Institute of Aquatic Science and Technology, Water Resources and Drinking Water, Ueberlandstrasse 133, 8600 Dübendorf, Switzerland
Received 2013 July 1; accepted 2013 September 25; published 2013 October 24

ABSTRACT

Recent work based on analyses of meteorite and terrestrial whole-rock samples showed that the r- and s- process isotopes of Hf were homogeneously distributed throughout the inner solar system. We report new Hf isotope data for Calcium-Aluminum-rich inclusions (CAIs) of the CV3 carbonaceous chondrite Allende, and novel high-precision Zr isotope data for these CAIs and three carbonaceous chondrites (CM, CO, CK). Our Zr data reveal enrichments in the neutron-rich isotope ^{96}Zr ($\leqslant 1\varepsilon$ in ^{96}Zr/^{90}Zr) for bulk chondrites and CAIs ($\sim 2\varepsilon$). Potential isotope effects due to incomplete sample dissolution, galactic and cosmic ray spallation, and the nuclear field shift are assessed and excluded, leading to the conclusion that the ^{96}Zr isotope variations are of nucleosynthetic origin. The ^{96}Zr enrichments are coupled with ^{50}Ti excesses suggesting that both nuclides were produced in the same astrophysical environment. The same CAIs also exhibit deficits in r-process Hf isotopes, which provides strong evidence for a decoupling between the nucleosynthetic processes that produce the light ($A \leqslant 130$) and heavy ($A > 130$) neutron-rich isotopes. We propose that the light neutron-capture isotopes largely formed in Type II supernovae (SNeII) with higher mass progenitors than the supernovae that produced the heavy r-process isotopes. In the context of our model, the light isotopes (e.g. ^{96}Zr) are predominantly synthesized via charged-particle reactions in a high entropy wind environment, in which Hf isotopes are not produced. Collectively, our data indicates that CAIs sampled an excess of materials produced in a normal mass (12–25 $M_{\odot}$) SNII.

Key words: meteorites, meteors, meteoroids – nuclear reactions, nucleosynthesis, abundances – stars: abundances – supernovae: individual: SNeII

1. INTRODUCTION

The primary elemental abundances of our solar system are the result of a multitude of complex nuclear processes that took place deep inside or in the envelope of different types of stars, which were averaged over the history of the Galactic evolution. Eight nuclear processes (H, He, s-, r-, p-, e- α-, and x-) were originally predicted by Burbidge et al. (1957) to complement the initial production of H, He, and small amounts of Li moments after the Big Bang (Gamow 1946; Alpher et al. 1948). Of these eight processes, the two neutron-capture processes—s(low) and r(apid)—are largely responsible for the production of heavy nuclides beyond Fe (Burbidge et al. 1957; Cameron 1957). The s-process takes place in the thermally pulsating asymptotic giant branch (TP-AGB) phases of low (1.5–3 $M_{\odot}$) and intermediate (5–8 $M_{\odot}$) mass stars (Arlandini et al. 1999; Gallino et al. 1988; Gallino et al. 1998; Meyer 1994), and the advanced evolutionary phases of more massive (>15 $M_{\odot}$) stars (Travaglio et al. 2004; Käppeler et al. 1989). The exact astrophysical site(s) and production mechanism(s) of the r-process, however, are yet to be determined (e.g., Wasserburg & Qian, 2009). Important constraints on the r-process mechanism and site can be gained from the analyses of (1) *elemental* abundance patterns of ultra-metal poor stars from spectral observations and (2) the *isotopic* compositions of primitive meteorites and their components (e.g., Sorlin et al. 2003; Birck 2004; Davis 2004; Lauretta & McSween 2006). Presolar grains, for example, that exist in these meteorites exhibit specific isotopic patterns, which reflect the nucleosynthetic fingerprint of their stellar production site (e.g., Zinner 2007).

A recent study (Sprung et al. 2010) indicates that Hf isotopes ($Z = 72$) are homogeneously distributed in the solar system at a bulk rock scale based on analyses of Calcium-Aluminum-rich inclusions (CAIs) from the carbonaceous chondrite Allende (CV3), various carbonaceous chondrites, and terrestrial samples. This homogeneity is in line with the reported s- and r-process homogeneity for Nd ($Z = 60$) and Sm ($Z = 62$) isotopes (Andreasen & Sharma 2007; Carlson et al. 2007), indicating that phases carrying s- and r-process isotopes were well-mixed in the solar nebula from which our solar system formed. In contrast to this evidence, Ba isotopes ($Z = 56$) show well resolved r-process heterogeneities in carbonaceous chondrites and this was taken as evidence for two distinct r-processes—one for light ($Z \leqslant 56$) and one for heavy ($Z > 56$) nuclei (Andreasen & Sharma 2006, 2007) that contributed to solar system materials.

Wasserburg et al. (1996) arrived at the same conclusion based on other meteoritic evidence. They showed that the initial solar system abundances of the *short-lived* radionuclides ^{129}I ($T_{1/2} =$ 16 Myr) and ^{182}Hf ($T_{1/2} = 9$ Myr), which are predominantly r-process isotopes, cannot be explained by a single supernova event. Instead, they proposed distinct r-process sources for the synthesis of light ($A < 130$, $Z \approx 56$) and heavy nuclei ($A > 130$, $Z \approx 56$), which require core-collapse Type II supernovae (SNeII) events with different mass progenitors acting on varying galactic timescales. Further studies (Qian et al. 1998, Wasserburg & Qian 2000a, 2000b, Wasserburg & Qian 2009) attributed the production of the light elements (L component; $Z < 56$) to normal mass (12–25 $M_{\odot}$), low frequency (timescale $\sim 10^8$ yr) SNeII, and the production of heavier elements (H component; $Z \geqslant 56$) to low mass (8–11 $M_{\odot}$), high frequency (timescale $\sim 10^7$ yr) SNeII.

Other evidence for a decoupling of r-process nucleosynthesis comes from spectroscopic observations of ultra-metal-poor stars. For example, studies of the ultra-metal-poor halo star CS

Table 1
Zr Isotope Yields from s-process Models

Isotope	Solar Abundance[a]	Main s-process			GCE[d]		Weak s[e]
		Stellar Model[b]	Classical Model[b]	Stellar Model[c]	IM	LM + IM	
^{90}Zr	51.45%	76%	72%	85%	6%	53%	2%
^{91}Zr	11.23%	102%	100%	106%	18%	80%	3%
^{92}Zr	17.14%	99%	108%	101%	15%	76%	3%
^{94}Zr	17.38%	114%	116%	126%	9%	79%	2%
^{96}Zr	2.80%	58%	53%	51%	40%	82%	0%

Notes.
[a] Updated solar system isotopic abundances from Lodders et al. (2009), expressed as percentages of the total elemental abundance.
[b] Stellar and classical model contributions to the main s-process from low mass AGB stars—Arlandini et al. (1999).
[c] Updated stellar model contributions to the main s-process from low mass AGB stars—Bisterzo et al. (2011).
[d] Galactic chemical evolution (GCE) of the main s-process from low (LM) and intermediate (IM) mass AGB stars—Travaglio et al. (2004). The GCE model incorporates LM AGB star yields from Arlandini et al. (1999).
[e] Weak s-process contribution from massive stars—Raiteri et al. (1993).

22892–052 reveal that this star is rich in neutron-capture elements (in particular Th, Os, and the second neutron-capture peak elements Ba, La, Ce, and Pr) relative to the Fe peak elements (Cowan et al. 1995; Sneden et al. 1996). This abundance pattern is characteristic for r-process nucleosynthesis. The occurrence of r-process nucleosynthesis in very old stars (e.g. CS 22892–052; age $\approx 14 \pm 3$ Gyr; Sneden et al. 2003) provides evidence that the r-process takes place in stars with very short evolutionary timescales, and therefore high masses ($M \geqslant 8\,M_{\odot}$; Cowan et al. 1995). Further studies showed that the elemental abundance pattern of the neutron-capture elements of many metal-poor stars (including CS 22892–052) match the scaled solar system r-process distribution for elements from Ba to Pb ($56 \leqslant Z \leqslant 82$; Sneden et al. 2003; Burris et al. 2000; Honda et al. 2004). The close match between these abundance patterns implies a uniform site or set of conditions for the r-process synthesis of heavy ($56 \leqslant Z \leqslant 82$) elements (Cowan et al. 1995; Sneden et al. 1996, 2000, 2003). However, the abundances of the lighter elements ($38 \leqslant Z \leqslant 56$) are underproduced relative to the heavy elements and deviate from a scaled solar system r-process distribution. This provides evidence for the existence of at least two distinct r-process sources: a main r-process source (synthesizing all r-nuclides) and an additional weak r-process (producing r-nuclides up to Ba; $Z = 56$). Noteworthy, the term *weak r-process* is not clearly defined. Kratz et al. (2008) argued that the mass region between Fe and Zr, which was historically thought of as the beginning of the weak r-process, is dominated by charged-particle reactions (CPRs) in the neutrino-driven wind of an SNII, whereas Travaglio et al. (2004) associated it with the lighter element particle process (LEPP) occurring in all massive stars.

In summary, various evidence supports the decoupling of nucleosynthetic sources at $Z = 56$. However, the sites of the two r-process components ($Z \leqslant 56$ and $Z > 56$) and in particular the nature of the low mass component ($Z \leqslant 56$) are still enigmatic. To determine the origin and degree of the decoupling of heavy and light nuclei, we performed high-precision isotope analyses for the intermediate mass element Zr ($Z = 40$) on the same digestions of CAIs, bulk meteorites, and terrestrial rocks that had previously been analyzed (Sprung et al. 2010) for the isotopic composition of the high mass element Hf ($Z = 72$). In addition, we report new Hf isotope data for additional Allende CAIs and a set of terrestrial igneous rock standards.

Only limited high-precision Zr isotope data for solar system materials are available so far. Isotopic variations in ^{96}Zr were identified for refractory inclusions of Allende (Harper et al. 1991; Schönbächler et al. 2003), whereas CV3 bulk carbonaceous chondrites showed hints of ^{96}Zr excesses that could not be entirely resolved (Schönbächler et al. 2003, 2005). Since the Zr isotopes are at the lower limit of the low mass r-process component, as determined by spectroscopic observations ($Z \sim 38$), the characterization of Zr isotope heterogeneities in solar system materials sheds light on the issue of whether heterogeneities in this mass range are generated by (1) r-process nuclei (low mass r-process component, SNII) also referred to as the weak r-process, (2) nuclei produced by CPRs in the neutrino-driven wind (SNII), or (3) nuclear statistical equilibrium (NSE) reactions that synthesized the neutron-rich isotopes (e.g., ^{48}Ca, ^{50}Ti, ^{54}Cr, ^{64}Ni, and ^{66}Zn) of the Fe group nuclei ($20 \leqslant Z \leqslant 30$), presumably in Type Ia supernovae (SNeIa; Meyer 1994).

Zirconium is part of the first s-process peak ($38 \leqslant Z \leqslant 40$), and its isotopic composition is largely the result of neutron-capture processes. Four isotopes (^{90,91,92,94}Zr) are mainly synthesized at low neutron exposures (neutron density: $N_n \leqslant 3\times10^7$ cm^{-3}), which are primarily generated by the ^{13}C(α,n)^{16}O neutron source at moderate stellar temperatures (kT $\sim$ 8 keV; Gallino et al. 1988; Arlandini et al. 1999). This source is active during recurring thermal instabilities in the H–He intershell of low (1.5–3 $M_{\odot}$) and intermediate (5–8 $M_{\odot}$) mass asymptotic giant branch (AGB) stars (Table 1). Collectively, these two sites constitute the main s-process. The weak s-process, which takes place in massive stars (>15 $M_{\odot}$), contributes a small fraction to these isotopes (Raiteri et al. 1993). A small proportion of ^{90}Zr is also produced by the p-process (Travaglio et al. 2011). The isotope ^{96}Zr, however, also originates from different nucleosynthetic sources compared to the other Zr isotopes. The relatively short beta-decay half-life of ^{95}Zr ($T_{1/2} = 64$ days) entails that only higher neutron fluxes ($N_n \geqslant 3\times10^8$ cm^{-3}; Lugaro et al. 2003; Nicolussi et al. 1997) lead to the production of ^{96}Zr. Traditionally, ^{96}Zr was considered an r-only isotope (Cameron 1973, Käppeler et al. 1989), whereas the most recent predictions (e.g., Bisterzo et al. 2011, Arlandini et al. 1999) for low mass (1.5–3 $M_{\odot}$) AGB stars estimate an r-process component that accounts for up to 49% of the total ^{96}Zr inventory in our solar system. A different approach considers the Galactic Chemical Evolution (GCE) of both low (1.5–3 $M_{\odot}$) and intermediate mass (5–8 $M_{\odot}$) AGB stars, with varying metallicities and ^{13}C pocket efficiencies (Travaglio et al. 2004). Particularly in intermediate-mass AGB stars, temperatures deep inside the convective region of the TP phase can reach

kT ~ 23 KeV, triggering a second neutron burst (maximum $N_n = 2\times10^{11}$ cm^{-3}; Lugaro et al. 2003) by the activation of the ^{22}Ne(α,n)^{25}Mg reaction. This results in a substantial ^{96}Zr production (40%; Table 1). Combined with the ^{96}Zr yields from low mass AGB stars, Travaglio et al. (2004) attributed 82% of the solar system ^{96}Zr to the s-process (Table 1), leaving 18% to other processes as, e.g., the r-process. In addition, alternative production sites for ^{96}Zr have been proposed. (1) Travaglio et al. (2004) suggested that the production of ^{96}Zr could be associated with the LEPP. This process is presumed to take place in massive ($M \geqslant 8\,M_{\odot}$) stars and contributes to the light elements only. (2) Neutron bursts, which occur in high temperature regions of SNeII, were also put forward to produce ^{96}Zr (Meyer et al. 2000). (3) Travaglio et al. (2011) showed that some ^{96}Zr may be synthesized alongside p-process isotopes in SNeIa.

Presolar grains provide further evidence for the specific production of ^{96}Zr. The majority of presolar SiC grains (mainstream grains) and most presolar graphite grains display depletions in ^{96}Zr relative to the other Zr isotopes (Nicolussi et al. 1997, Davis et al. 1999b, Nicolussi et al. 1998). These grains experienced relatively low neutron exposures and were thus unable to bypass the bottleneck at ^{95}Zr and produce ^{96}Zr. This is in agreement with formation around low mass AGB stars (Anders & Zinner, 1993). A small fraction (~1%) of SiC grains—Type X grains—exhibit strongly enhanced ^{96}Zr abundances. These enrichments match the predictions of neutron-burst models in a supernova environment (Pellin et al. 2006). A small fraction of the presolar graphite grains are also characterized by enrichments in ^{96}Zr, pointing to either a high-density s-process in AGB stars or r-process nucleosynthesis in core-collapse SNe (Nicolussi et al. 1998). Whichever production site (and mechanism) is relevant for the average solar system Zr isotope composition, it is evident that a significant fraction of ^{96}Zr is synthesized in more energetic environments than the other Zr isotopes and can therefore serves as fingerprint of such nucleosynthetic sites.

The comparison of Zr with Hf isotopes is powerful because Zr and Hf share many similarities, but also lie on either side of the proposed r-process mass-cut at $Z = 56$. Hafnium possesses two mainly s-process isotopes—^{178}Hf (59%, s-process), ^{180}Hf (89%, s-process)—and two dominantly r-process isotopes—^{177}Hf (83%, r-process) and ^{179}Hf (59%, r-process; Bisterzo et al. 2011). The two elements also display comparable electron configurations (group IV) and ionic radii ($r^{4+}_{[Zr,Hf]} \sim 79$ pm), and form similar oxides. This, combined with their highly refractory nature (half mass condensation temperature $T_c^{[Zr]} = 1764$ K, $T_c^{[Hf]} = 1703$ K; Lodders 2003), results in almost identical geochemical and cosmochemical behaviors of the two elements. Therefore, only limited fractionation is expected between the two elements during the physical and chemical processing that they may have experienced after their synthesis when they were situated in their presolar phases or later during solar system formation and parent body processing. In conclusion, combined isotopic measurements of both Zr and Hf represent a unique and powerful tool for assessing the decoupling of the variable nucleosynthetic sources that produced the light and heavy nuclei.

In this study, we present and compare high-precision Zr and Hf isotope data for CAIs, carbonaceous chondrites, and terrestrial samples. The Hf isotope analyses follow the procedure of Sprung et al. (2010), while the Zr analyses are based on the analytical techniques developed by Schönbächler et al. (2004). In particular, the anion exchange procedure of Schönbächler et al. (2004) was modified and different digestion techniques were applied to determine the effects of incomplete sample dissolution on the Zr isotope composition of carbonaceous chondrites. Our study reveals clearly resolved enrichments in the neutron-rich isotope ^{96}Zr in bulk carbonaceous chondrites and Allende CAIs compared to terrestrial samples. Of these CAIs, all but two also display r-process deficits for Hf, which is—to our knowledge—the first time that nucleosynthetic isotope anomalies are reported for Hf in material other than presolar grains (Yin et al. 2006). The results are consistent with two distinct nucleosynthetic processes for the production of neutron-rich isotopes, operating in different mass regimes (corresponding to $Z \leqslant 56$ and $Z > 56$), and the ^{96}Zr production via CPRs in an SNII.

2. EXPERIMENTAL

Approximately 1g of Murchison (CM2) was powdered in an aluminum oxide mortar and pestle. The powder was subjected to three different digestion techniques: (a) hotplate, (b) microwave, and (c) Parr© bomb acid digestions. For the hotplate digestion, up to 1 g of powdered sample was placed inside a Savillex vial, with concentrated HF–HNO_3 (2:1, 15 ml; Schönbächler et al. 2004) The vial was heated to 150 °C during 48 hours. For the microwave digestions, up to 300 mg of powdered Murchison was placed inside a pre-cleaned Teflon microwave digestion vessel, with 10 ml concentrated HF, 3 ml concentrated HNO_3 and 2 ml de-ionized water (18.2 MΩ·cm). The microwave vessels were sealed in a laboratory grade microwave and pre-programmed with 1 run consisting of a 15 minute ramp to a pressure of 100 PSI, a 15 minute hold at 100 PSI, and a 30 minute de-pressurization and cooling stage. For the Parr bomb digestion, 300 mg of the sample was weighed into a pre-cleaned 15 ml Savillex beaker, to which 3 ml concentrated HF and 100 μl concentrated HNO_3 was added. The beaker was sealed in a Parr acid digestion vessel for 108 hours at 170 °C (as described in Schönbächler et al. 2004). Following the digestion procedure, the samples were dried down at 80 °C. If any organic material remained, aqua regia was added (3:1 HCl:HNO_3; 6 ml) for 24 hours at 120 °C on a hotplate. All samples (hotplate, microwave, or Parr bomb digested) were finally refluxed in 5 ml of 6 M HCl at 120 °C for 48 hours.

Three CAIs (CAI_NV_1, CAI_NV_2, and CAI_NV_3) were separated from Allende (CV3) using a micro drill (Preiswerk 2011), and digested in the Parr bomb. Two CAIs (CAI_PS_2 and CAI_PS_4) were digested using the Parr bomb technique outlined in Sprung et al. (2010), and two additional CAIs (CAI_PS_1 and CAI_PS_5) were digested in 15 ml Savillex vials for 24 h on a hotplate at 120 °C using 8 ml of concentrated HF–HNO_3 (3:1).

The Zr fractions of samples that were previously analyzed for Hf isotopes (Sprung et al. 2010) were also analyzed. The sample set included a terrestrial andesite (AGV-2), three whole-rock carbonaceous chondrites—Murchison (CM2), Dar al Gani 137 (CO3), Dar al Gani 275 (CK4/5), and two Allende CAIs (CAI_PS_2, CAI_PS_4). Details of the sample preparation, digestion method, and initial chemical separation of Hf and Zr from the sample matrix are given in Sprung et al. (2010).

The chemical separation of Zr from the sample matrix followed the two-stage anion exchange technique developed by Schönbächler et al. (2004). The first stage employs AG1 X8 anion exchange resin (200–400 mesh, Cl-form) in combination with HF and HCl. The second stage uses 0.25 M H_2SO_4–1% H_2O_2 for sample loading and matrix elution. An additional step involving 2 ml 0.5 M HCl–0.5 M HF was introduced to improve

Table 2
Zirconium Isotope Compositions of Murchison (CM2) for Different Digestion Techniques

Digestion Method	ε^{91}Zr	ε^{92}Zr	ε^{96}Zr	n
Hotplate	-0.11 ± 0.14	-0.23 ± 0.11	1.95 ± 0.33	1
Microwave	-0.27 ± 0.14	-0.11 ± 0.10	0.19 ± 0.36	1
Parr bomb	0.02 ± 0.06	0.02 ± 0.06	0.86 ± 0.18	6
Parr bomb[a]	0.0 ± 0.4	0.1 ± 0.3	0.9 ± 1.6	4

Notes.
For repeat measurements, the weighted average of each group is shown, along with the associated weighted mean uncertainties (2σ), otherwise the internal uncertainty (standard error of the mean for 60 ratios per measurement) is given. Four of the six Parr bomb measurements are replicate analyses of a Zr fraction obtained from a digestion performed at the Universität Münster. The remaining two data points are replicate analyses of a Zr fraction obtained from a different chip of the Murchison meteorite (processed at The University of Manchester).
[a] Data from Schönbächler et al. (2005).

the removal of remaining traces of H_2SO_4 before the elution of Zr in 6 M HCl–1 M HF from the column (Akram 2013).

Zirconium fractions obtained from a previous study (Sprung et al. 2010) were passed through an additional anion exchange column (first stage from Schönbächler et al. 2004) to ensure the adequate removal of Zr from the sample matrix.

Following the anion exchange procedure, the Zr fractions were evaporated and dissolved in 0.5 M HNO_3—0.005 M HF for multiple collector—inductively coupled plasma mass spectrometer (MC-ICPMS) analysis. A 2% aliquot of each sample was screened prior to the Zr isotope measurements to ensure that the levels of interfering isobars (^{94,96}Mo, ^{96}Ru), argides (^{50}Ti^{40}Ar, ^{51}V^{40}Ar, ^{52}Cr^{40}Ar, ^{54}Fe^{40}Ar), and double charged species (180Hf^{++}, 182W^{++}, 184W^{++}) remained within acceptable limits (Mo/Zr = 0.001, Ru/Zr = 0.01, Ti/Zr = 1, V/Zr = 0.3, Cr/Zr = 0.3, Fe/Zr = 0.9; Schönbächler et al. 2004). If the concentrations of interfering species exceeded the limits, the ion exchange procedure was repeated for the respective sample.

The Zr isotopic analyses were carried out on a Nu Plasma MC–ICPMS at The University of Manchester, coupled with an Aridus II nebuliser sample injection system. All five Zr isotopes were simultaneously analyzed on different Faraday collectors. The signal intensities were normalized to ^{90}Zr and corrected for instrumental mass bias relative to ^{94}Zr/^{90}Zr = 0.3381 (Minster & Ricard 1981) using the exponential law. Additional isotopes (^{95}Mo, ^{99}Ru) were also monitored to correct for isobaric interferences on ^{92}Zr (^{92}Mo), ^{94}Zr (^{94}Mo), and ^{96}Zr (^{96}Mo, ^{96}Ru), using a second cycle (cycle 1: mass 90–96; cycle 2: mass 95–101). Individual sample measurements consisted of 5 s integrations repeated 60 times. Electronic baselines were measured before each analysis for 15 s. All samples were bracketed by a synthetic Zr Alfa Aesar standard solution, at ion beam intensities that were matched to better than 20%. Depending on the daily sensitivity, 200–400 ng of Zr was needed per measurement and this yielded total Zr ion beam intensities between 2.5×10^{-10} A and 3.5×10^{-10} A (using amplifiers running at $10^{11}\Omega$). The Zr isotope ratios of samples are expressed as the deviation from the Alfa Aeser Zr standard solution (i.e., the terrestrial composition) in parts per ten thousand (ε).

New Hf isotope data is presented for CAI_NV_1, CAI_NV_2, CAI_NV_3, CAI_PS_1, and CAI_PS_5. The powder aliquots for CAI_NV_1, CAI_NV_2, and CAI_NV_3 were first laser-fused (Pack et al. 2010) and then digested for 24 h at 120 °C in 15 ml Savillex vials using 8 ml of concentrated HF–HNO_3 (3:1). The chemical separation procedure of Hf and the mass spectrometric analysis are described in Sprung et al. (2010, 2013). The Hf data (this study) are reported relative to the isotopic compositions of terrestrial rock standards that were obtained during the same measurement sessions. This is different to Sprung et al. (2010), where an Ames Hf solution standard was used. The new method compensates for a bias on ε^{178}Hf (Sprung et al. 2010) observed for terrestrial rocks relative to the Ames Hf standard solution. The Hf isotope compositions are corrected for instrumental mass fractionation relative to the two dominantly s-process isotopes (^{178}Hf/^{180}Hf) or the two dominantly r-process isotopes (^{179}Hf/^{177}Hf), yielding ε^{177}Hf$_s$ and ε^{179}Hf$_s$ or ε^{178}Hf$_r$ and ε^{180}Hf$_r$, respectively. The subscripts on ε identify whether the normalization to the s-process (s) or r-process (r) Hf isotopes is used.

3. RESULTS AND DISCUSSION

3.1. Dissolution of Refractory Presolar Phases in Murchison (CM2)

The hotplate digestion yields a positive ε^{96}Zr of +1.95 ± 0.33 (Figure 1, Table 2), which is significantly higher than the results obtained by other digestion techniques (Parr bomb and microwave). The results for ε^{91}Zr and ε^{92}Zr are broadly similar for all digestion methods within the quoted uncertainties at the 3σ level. The difference in ε^{96}Zr between hotplate and Parr bomb (or Microwave) digestions most likely results from an incomplete dissolution of refractory carriers of anomalous Zr (e.g., presolar grains) in carbonaceous chondrites by hotplate digestions. Murchison contains a significant fraction of presolar silicon carbide (SiC) grains (9 ppm; Huss 1997), which are known to be chemically resilient (Amari et al. 1995; Merchel et al. 2003; Brandon et al. 2005). The bulk of these grains (⩾90%; Lugaro et al. 2003) belong to the group of mainstream grains. These grains are abundant in Zr, with concentrations varying with grain size fractions (KJA (0.05–0.1 μm): 1100 ppm, KJB (0.1–0.2 μm): 700 ppm, KJC (0.2–0.3 μm): 500 ppm, KJD (0.3–0.5 μm): 1200 ppm, KJE (0.5–0.8 μm): 1600 ppm, KJF (0.8–1.5 μm): 500 ppm, KJG (1.5–3 μm): 80 ppm, KJH (3–5 μm): 80 ppm; Amari et al. 1995). They are enriched in the s-process isotopes (^{90,91,92,94}Zr) by up to 1000ε, but depleted in ^{96}Zr (–5000 to –10,000 ε), when normalized to either ^{90,91,92,94}Zr (Nicolussi et al. 1997; Davis et al. 1999a, 1999b) relative to the Earth. These grains therefore contribute a negative ε^{96}Zr component to the bulk rock composition of Murchison. Incomplete dissolution (extraction) of these grains consequently leads to a positive ε^{96}Zr for whole-rock analyses of Murchison. The SiC grains can account for up to 10ε in ^{96}Zr/^{90}Zr (Schönbächler et al. 2005).

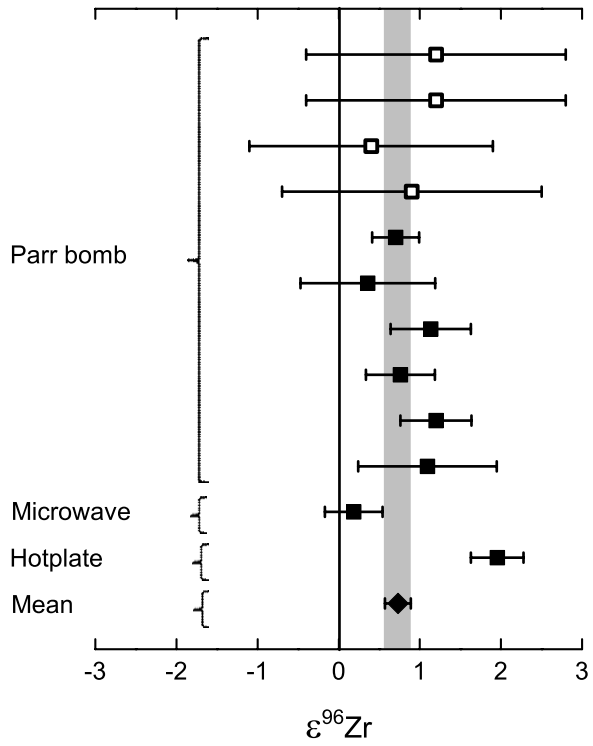

Figure 1. ε^{96}Zr data for different digests of Murchison. The gray bar denotes the weighted mean uncertainty (2σ) of the Parr bomb and microwave digestions. Data from this study (filled squares) and from Schönbächler et al. 2005 (open squares).

The measured ε^{96}Zr value of the hotplate digested Murchison (1.95 ± 0.33) is within this range, and suggests that the relatively low pressure environment provided by the hotplate digest is insufficient to completely dissolve SiC grains. In contrast, leaching (Schönbächler et al. 2005) and SiC grain extraction experiments (Merchel et al. 2003) showed that Parr bomb and microwave digestions dissolve SiC grains. These findings are in line with the nearly identical Zr isotope compositions that were obtained for microwave and Parr bomb digestions of Murchison (Table 2). Both methods are thus considered to provide similar digestion efficiencies for Zr bearing phases in carbonaceous chondrites. This may not necessarily apply to other elements. For example, recent experiments, which compared hotplate and laser fusion digestions of Murchison (Burkhardt et al. 2011), revealed identical Mo isotope compositions. Burkhardt et al. (2011) used perchloric acid ($HClO_4$) in addition to the HNO_3–HF mixture for their hotplate digestion, which may have yielded a more complete digestion of refractory grains. It is also possible that Mo, due to its redox sensitivity, is more easily leached from SiC grains than Zr. This would render a Parr bomb digestion for Mo isotopes unnecessary, while being mandatory for Zr isotopes.

In this study, only Zr data from carbonaceous chondrites that were digested in Parr bombs are considered for the further discussion to avoid artifacts due to incomplete digestion of refractory presolar phases. It is noteworthy that Murchison still shows a resolvable, positive ε^{96}Zr (+0.86 ± 0.18; Table 2) after excluding the effects ascribed to incomplete dissolution. Interestingly, all ε^{177}Hf$_s$, ε^{179}Hf$_s$, (ε^{178}Hf$_r$, ε^{180}Hf$_r$), and ε^{96}Zr values obtained for the hotplate-digested CAIs (CAI_PS_1 and CAI_PS_5) are in excellent agreement with the data obtained for CAIs, which were digested using Parr bombs (Zr) or laser-fused (Hf) (CAI_PS_2, CAI_NV_1, CAI_NV2; Table 3). Any potential bias resulting from an incomplete digestion of these CAIs is thus insignificant.

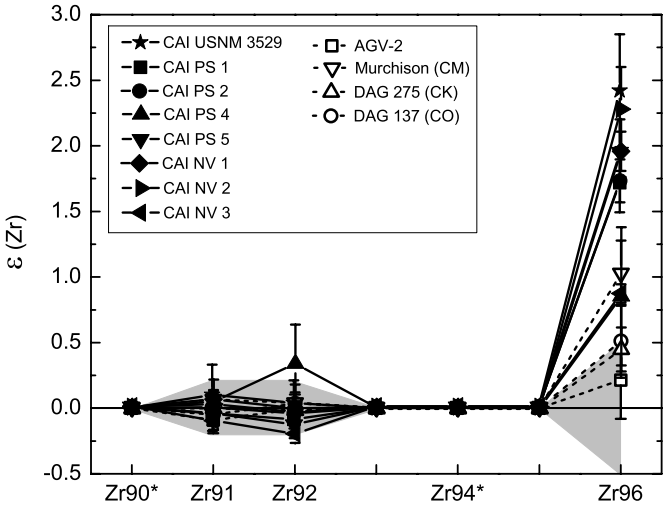

Figure 2. Zirconium isotope compositions of CAIs, terrestrial and carbonaceous chondrite bulk-rock samples. The isotopes are normalized to ^{94}Zr/^{90}Zr (indicated by an asterisk). For repeat measurements, the weighted mean and its associated uncertainty (2σ) are shown, otherwise the internal error is given. Dark bands show the long-term reproducibility (standard deviation, 2σ) of the terrestrial standards.

3.2. Origin of Zr Isotope Heterogeneities: Nucleosynthesis, Cosmic Ray Irradiation, or Nuclear Field Shift?

Carbonaceous chondrites, which within uncertainty possess a terrestrial Hf isotope composition (Sprung et al. 2010), display Zr isotope compositions different from the Earth (Figure 2; Table 3). The excesses in the neutron-rich isotope ^{96}Zr range up to 1ε for bulk samples of carbonaceous chondrites. The ^{96}Zr/^{90}Zr excess in Murchison (CM2; Tables 2 and 3) is in good agreement with previous measurements (Schönbächler et al. 2003). However, Schönbächler et al. (2003) were not able to resolve the difference between carbonaceous chondrites and the terrestrial standard because of the lower analytical precision. The ^{96}Zr/^{90}Zr enrichments in Dar al Gani 137 (CO) and Dar al Gani 274 (CK) currently overlap with the upper limit ($\pm 0.54\varepsilon$) of the long term reproducibility (2σ standard deviation) of our terrestrial standards (Akram 2013). However, when compared to the weighted average ^{96}Zr/^{90}Zr values of our terrestrial rock standards ($\varepsilon^{96}\text{Zr} = 0.06 \pm 0.04$, 2σ; n = 67) determined over a period of two years (Akram 2013), the positive ε^{96}Zr values are clearly resolved. All CAIs show well-resolved excesses in ^{96}Zr. Previous excesses ($\varepsilon^{96}\text{Zr} = 1.9 \pm 1.4$) determined for CAI USNM 3529–41 (Schönbächler et al. 2003), were reproduced at higher precision ($\varepsilon^{96}\text{Zr} = 2.4 \pm 0.4$; Figure 3). The ^{96}Zr excesses are generally attributed to nucleosynthetic heterogeneities preserved in our solar system (Schönbächler et al. 2003, 2005). Other possibilities are cosmic ray irradiation by the early sun or effects due to the nuclear field shift (see below). Models calculating Zr isotope production by galactic and solar cosmic ray irradiation, however, showed that such effects are too small to significantly affect the abundances of Zr isotopes (Leya et al. 2003; Schönbächler et al. 2005). Similarly, irradiation effects are too small (Leya et al. 2009; Zhang et al. 2012) to account for the observed isotopic heterogeneity in Ti for carbonaceous chondrites (Leya et al. 2009; Trinquier et al. 2009).

Table 3
Zirconium and Hf Isotope Compositions of CAIs, Carbonaceous Chondrites and AGV-2.

Sample	Type	Zf/Hf	ε^{91}Zr	ε^{92}Zr	ε^{96}Zr	n	ε^{178}Hf [r]	ε^{180}Hf [r]	ε^{177}Hf [s]	ε^{179}Hf [s]	n
Bulk rock:											
AGV-2[†]	Andesite	45 [a]	-0.09 ± 0.10	-0.01 ± 0.11	0.22 ± 0.30	2	-0.04 ± 0.08	0.09 ± 0.11	0.03 ± 0.14	0.00 ± 0.12	7
Murchison[†]	CM2	31[b]	0.06 ± 0.07	0.04 ± 0.08	1.02 ± 0.25	4	-0.13 ± 0.10	-0.08 ± 0.22	-0.01 ± 0.16	0.08 ± 0.14	2
Dar al Gani 137[†]	CO3	...	-0.05 ± 0.12	0.03 ± 0.14	0.51 ± 0.28	1	-0.01 ± 0.18	0.04 ± 0.41	-0.18 ± 0.27	-0.05 ± 0.27	1
Dar al Gani 275[†]	CK4/5	...	0.00 ± 0.07	-0.01 ± 0.09	0.45 ± 0.17	3	-0.01 ± 0.18	0.24 ± 0.38	-0.08 ± 0.31	-0.16 ± 0.25	1
CAIs:											
CAI_PS_1[††]	Allende CAI	...	-0.04 ± 0.09	-0.09 ± 0.07	1.71 ± 0.22	4	0.21 ± 0.02	0.47 ± 0.13	-0.10 ± 0.07	-0.35 ± 0.07	8
CAI_PS_2[†]	Allende CAI	...	0.00 ± 0.07	-0.04 ± 0.05	1.74 ± 0.17	5	0.19 ± 0.16	0.38 ± 0.47	-0.21 ± 0.18	-0.24 ± 0.46	3
CAI_PS_4[†]	Allende CAI	...	0.05 ± 0.17	0.34 ± 0.30	0.85 ± 0.53	1	-0.33 ± 0.50	-0.75 ± 1.50	0.10 ± 0.29	0.27 ± 0.70	1
CAI_PS_5[††]	Allende CAI	...	-0.05 ± 0.14	-0.14 ± 0.11	1.95 ± 0.25	3	0.16 ± 0.02	0.33 ± 0.05	-0.07 ± 0.03	-0.24 ± 0.03	8
CAI_NV_1	Allende CAI	38[c]	0.06 ± 0.05	-0.01 ± 0.04	1.95 ± 0.15	6	0.19 ± 0.03	0.31 ± 0.04	-0.16 ± 0.06	-0.25 ± 0.03	7
CAI_NV_2	Allende CAI	41[c]	0.02 ± 0.10	-0.04 ± 0.07	2.27 ± 0.32	2	0.18 ± 0.07	0.28 ± 0.09	-0.17 ± 0.06	-0.23 ± 0.08	6
CAI_NV_3	Allende CAI	40[c]	-0.11 ± 0.07	-0.21 ± 0.07	0.86 ± 0.15	4	-0.10 ± 0.04	-0.16 ± 0.11	0.07 ± 0.07	0.13 ± 0.05	6
CAI USNM 3529–41	Allende CAI	36[d]	0.10 ± 0.23	0.04 ± 0.17	2.42 ± 0.43	1	...	...	...	...	...

Notes.
The weighted mean Zr isotope composition normalized to ^{94}Zr/^{90}Zr and the associated 2σ uncertainty are shown for repeat measurements. For single measurements (n = 1), the internal uncertainty of the measurement is propagated (in quadrature) with the uncertainty on the Alfa Aesar bracketing standards obtained during the same analytical session. All Zr isotope data from this study. The Hf isotope data are corrected for instrumental mass bias relative to the two dominantly r-process isotopes, ^{177}Hf/^{179}Hf (denoted [r], following Sprung et al. 2010) and were renormalized to the two dominantly s-process isotopes ^{178}Hf/^{180}Hf (denoted [s]). All Hf data (this study; Sprung et al. 2010) are corrected for a possible offset in ε^{178}Hf, by normalizing the data relative to the average Hf isotope composition of all terrestrial rock standards ran in the same analytical session. For repeat measurements of the same sample, the arithmetic mean and the error on the mean is given (using the Student's t-factor distribution, 95% confidence level) in accordance with Sprung et al. (2010). For the Hf isotope composition of Murchison (n = 2), the weighted average and its associated uncertainty (2σ) is given.
[†] Hf isotope data from Sprung et al. (2010).
[††] Samples are corrected for a minor Hf spike contamination (i.e. correction on ε^{178}Hf < 1 ppm). The uncertainty of the correction is included into the quoted uncertainties. (a) Wilson (1998). (b) Patzer et al. (2010). (c) Preiswerk (2011). (d) Mason & Taylor (1982).

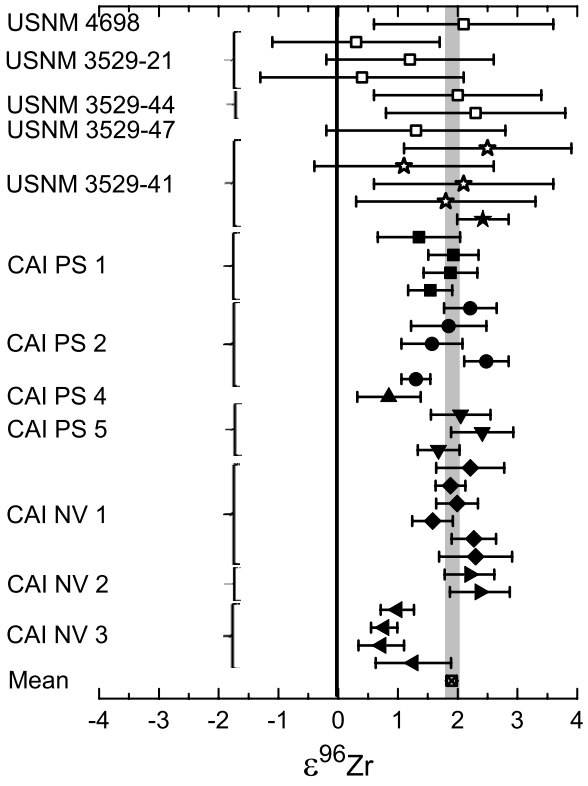

Figure 3. Zirconium isotope compositions of CAIs. Individual ε^{96}Zr values for repeat measurements of Allende CAIs (2σ uncertainties). The weighted mean of all CAIs analyzed in this study (excluding CAI_PS_4 and CAI_NV_3) is represented by the label Mean. Open symbols (Schönbächler et al. 2004), closed symbols (this study).

Alternatively, the mass-independent isotope effects in meteorites could arise from the nuclear volume field shift (Fujii et al. 2006). The addition of neutrons to a nucleus changes the nuclear volume and consequently the electrostatic charge distribution of the nucleus. This change alters the atomic energy transitions of the inner s and p shell electrons (Bigeleisen 1996). In principle, such nuclear volume variations can induce isotopic fractionation as a function of differing bonding energies (Fujii et al. 2006). The contribution of the field shift to a given isotope ratio (i/j), relative to the normalization pair (k/j) used to correct for instrumental mass fractionation, expressed in epsilon ($\varepsilon^{i/j}_{FS}$) is given by Equation (1) from Fujii et al. (2006):

$$\varepsilon^{i/j}_{FS} = \left[\delta\langle r^2\rangle_{m_j,m_i} \frac{m_k(m_i - m_j)}{m_i(m_k - m_j)} \delta\langle r^2\rangle_{m_j,m_k}\right] a. \quad (1)$$

The masses and changes in the mean square radius of two nuclei (i, j) are denoted by m and $\delta\langle r^2\rangle_{mi,mj}$, respectively. This equation was applied to Zr isotopes (Table 4), using the standard normalization scheme (^{94}Zr/^{90}Zr) and adopting the nuclear masses and mean square nuclear radii from Minster & Allègre (1982) and Angeli (2004). The dependence on a can be removed by calculating the ratio of any two relative field shift epsilon values and results in $\varepsilon^{96}_{FS}/\varepsilon^{91}_{FS} \sim +9$, $\varepsilon^{96}_{FS}/\varepsilon^{92}_{FS} \sim -2$, $\varepsilon^{92}_{FS}/\varepsilon^{91}_{FS} \sim -4$ (Table 4). The comparison of the Zr isotope compositions for the CAIs ($\varepsilon^{96}_{CAI}/\varepsilon^{91}_{CAI} \sim +62$, $\varepsilon^{96}_{CAI}/\varepsilon^{92}_{CAI} \sim -62$, $\varepsilon^{92}_{CAI}/\varepsilon^{91}_{CAI} \sim -1$) with the predicted field shift shows that the respective signs of the anomalies are reproduced correctly. However, the magnitude of the expected ε^{96}Zr anomaly, relative to ε^{91}Zr (i.e. $\varepsilon^{96}_{FS}/\varepsilon^{91}_{FS}$) is severely under-produced by almost one order of magnitude by the field shift calculations. In addition, the model predicts an ε^{92}Zr/ε^{91}Zr ratio of −4, while CAIs yield a ratio of −1 (Table 4).

Table 4
The Relative and Absolute Nuclear Field Shift for Zr Isotopes

	Field Shift $\varepsilon^{i}_{Zr}\|_{FS}$	Measured $\varepsilon^{i}_{Zr}\|_{CAI}$
Relative ε		
ε^{91}_{Zr}	$+0.010 \times a$	...
ε^{92}_{Zr}	$-0.039 \times a$	...
ε^{96}_{Zr}	$+0.087 \times a$	...
Absolute ε		
ε^{91}_{Zr}	+0.09	$+0.03 \pm 0.03$
ε^{92}_{Zr}	−0.33	-0.03 ± 0.03
ε^{96}_{Zr}	+0.73	$+1.90 \pm 0.09$
Nuclear masses[a]:		
$m(^{90}Zr) = 89.904708$, $m(^{91}Zr) = 90.9056442$, $m(^{92}Zr) = 91.9050392$, $m(^{94}Zr) = 93.9063191$, $m(^{96}Zr) = 95.908272$		

Notes.
The relative field shift (FS) is given in terms of the free parameter a, whereas the absolute field shift values are calculated for the optimized value of $a = 8.4$ (see text). Also shown are the weighted averages, and associated uncertainty (2σ) of the CAI Zr data for comparison (excluding CAI_NV_3 and CAI_PS_4; see Sections 3.3 and 3.4).
[a] Minster & Allègre (1982).

Alternatively, the absolute value of the field shift effect can be estimated semi-empirically by optimizing the parameter a to fit the absolute model predictions to the measured data (Table 4). This can account for up to 40% of the CAI ε^{96}Zr value, but for the same value of a, the model also predicts a lower, negative ε^{92}Zr by a factor of ∼11, which is not observed. Hence, the field shift fails to reproduce both the pattern and the magnitude of the anomalous Zr isotope composition of CAIs and is thus unlikely to be the major source for the ^{96}Zr excesses in meteorites. Our conclusion contrasts with the findings of Fujii et al. (2006), who explained the anomalous isotopic pattern of Ca, Ti, Cr, Sr, and Ba in FUN (Fractionated and Unknown Nuclear effects) CAIs with the field shift. Our results, however, are in line with the work of Brennecka et al. (2011), who applied the same technique to the Mo, Ba, Nd, and Sm isotope compositions of common CAIs and concluded that the effects induced by the field shift could not be solely responsible for the isotopic anomalies in CAIs. In summary, this leaves nucleosynthetic processes as the primary origin for the observed Zr anomalies.

3.3. Origin of Hf Isotope Heterogeneities in CAIs

Five CAIs yield resolvable, positive $\varepsilon^{178}Hf_r$ relative to the average composition of terrestrial rocks (Table 3). These $\varepsilon^{178}Hf_r$ are associated with positive, albeit not always resolved, $\varepsilon^{180}Hf_r$. Considering the s-process normalization relative to $^{178}Hf/^{180}Hf$, the data show resolved negative $\varepsilon^{179}Hf_s$ and $\varepsilon^{177}Hf_s$ values (for four and five CAIs, respectively; Table 3). Overall, these five CAIs display weighted average $\varepsilon^{177}Hf_s$, $\varepsilon^{179}Hf_s$, $\varepsilon^{178}Hf_r$, and $\varepsilon^{180}Hf_r$ values of –0.10 ± 0.02, –0.25 ± 0.02, +0.19 ± 0.01, and +0.32 ± 0.03, respectively. The data from both normalization schemes are consistent with a Hf r-process deficit (or s-process excess) that was sampled by CAIs. It is noteworthy that CAI_NV_3 and CAI PS_4 are different from the other CAIs and display positive $\varepsilon^{177}Hf_r$ and $\varepsilon^{179}Hf_r$, with weighted average values of 0.07 ± 0.07 and 0.13 ± 0.05, respectively. Hence, based on Hf isotopes, the analyzed CAIs can be divided into two groups. The observed Hf isotope variations are most likely due to nucleosynthetic effects. Secondary neutron-capture induced effects in Hf isotopes can be prominent but result in coupled $\varepsilon^{178,180}Hf_r$ (Sprung et al. 2010, 2013) that differ significantly from those observed in this study, i.e., positive $\varepsilon^{178}Hf_r$ associated with negative $\varepsilon^{180}Hf_r$. Moreover, Fujii et al. (2001) experimentally investigated Hf for nuclear field shift effects related to nuclear volume differences and concluded that they are insignificant.

3.4. Nucleosynthetic Zirconium Isotope Heterogeneities in Carbonaceous Chondrites and CAIs

While carbonaceous chondrites possess clearly resolved positive ε^{96}Zr (Figure 2; Table 3), CAIs from Allende yield the largest ^{96}Zr enrichments yet reported for solar system materials (Table 3). The most striking feature is the observation that most CAIs display identical $^{96}Zr/^{90}Zr$ enrichments with a weighted average of $\varepsilon^{96}Zr = +1.90 \pm 0.09$ (2σ weighted average uncertainty; Figure 3). The exceptions, which are thus not included in the mean, are CAI_NV_3 ($\varepsilon^{96}Zr = 0.86 \pm 0.15$) and CAI_PS_4 ($\varepsilon^{96}Zr = 0.85 \pm 0.53$), which define a weighted average of $\varepsilon^{96}Zr = 0.86 \pm 0.14$, ($2\sigma$). These are the same two CAIs that do not show negative $\varepsilon^{177}Hf_s$ and $\varepsilon^{179}Hf_s$ values. Similarly, Schönbächler et al. (2003) also identified CAI USNM 3529–21 and USNM 3529–47 with low positive ε^{96}Zr values, which correlate with low ε^{50}Ti (Leya et al. 2009) and ε^{62}Ni (Quitté et al. 2007) values. During the preparation of the CAIs, care was taken to ensure minimal contamination (approximately < 1%) from matrix material. Mass balance calculations show that contamination with 1% matrix material does not lead to a significant variation in the Zr isotope composition. Hence, matrix contamination cannot explain the low ε^{96}Zr values of CAI_NV_3, CAI_PS_4, CAI USNM 3529–21, and USNM 3529–47 (one-fourth of the analyzed CAIs).

The observation that the majority (75%) of the analyzed CAIs possess a virtually uniform Zr isotope composition suggests that most CAIs formed from a well-mixed isotope reservoir that is different compared to the average solar system composition. The variation in ε^{96}Zr does not correlate with petrographic type, rare earth element (REE) pattern, or degree of alteration (Schönbächler et al. 2003). Including the newly analyzed CAIs (using trace element data from Preiswerk 2011) this observation also holds true for Hf isotopes and indicates that the isotope variations are not the result of aqueous alteration nor related to the condensation and evaporation processes that lead to the formation of Type A or Type B CAIs. Therefore, the isotopic variations most likely reflect an original isotopic signature that CAIs inherited from sampling a specific mixture of gas and

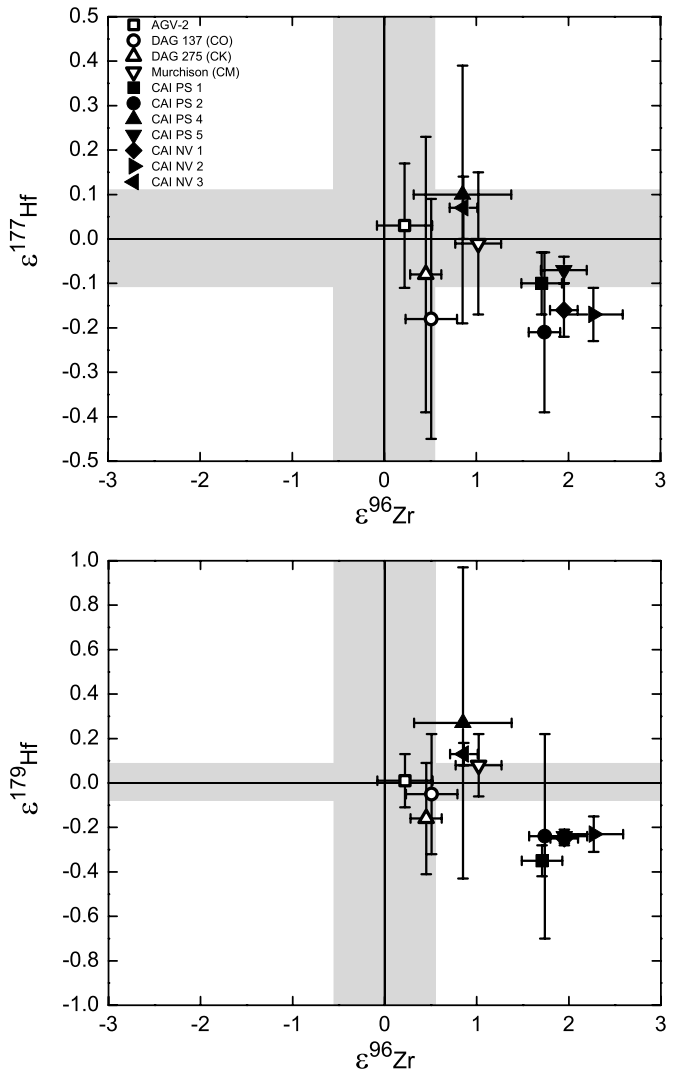

Figure 4. Four-isotope diagrams showing ε^{96}Zr vs. ε^{177}Hf and ε^{177}Hf for CAIs, carbonaceous chondrites, and a terrestrial sample (AGV-2). Data and uncertainties are from Table 3. Gray bands represent the long-term reproducibilities defined by the 2σ standard deviation of the terrestrial rock standards measured over 2 yr.

dust within the solar nebula. It is noteworthy that the positive ε^{96}Zr values correlate with the Hf isotope variations (Figure 4), with ε^{50}Ti (Leya et al. 2009; Harper et al. 1991), and ε^{62}Ni (Quitté et al. 2007). The majority of the CAIs display a uniform $\varepsilon^{50}\text{Ti} = +9.0 \pm 0.1$ (Leya et al. 2009; Trinquier et al. 2009) coupled with $\varepsilon^{96}\text{Zr} = 1.90 \pm 0.09$, $\varepsilon^{177}\text{Hf}_s = -0.10 \pm 0.02$ and $\varepsilon^{179}\text{Hf}_s = -0.25 \pm 0.02$. Therefore, this majority potentially condensed from a gas phase in an area in the solar nebula that was characterized by material with uniformly positive ε^{96}Zr, ε^{50}Ti, and negative $\varepsilon^{177,179}\text{Hf}_s$. The CAIs with lower ε^{96}Zr and ε^{50}Ti excesses and higher $\varepsilon^{177,179}\text{Hf}_s$ rather formed at the edge of this reservoir, sampling a larger amount of average solar system materials. However, the addition of terrestrial Hf ($\varepsilon^{177,179}\text{Hf}_s = 0$) to the bulk of the CAIs (with $\varepsilon^{177,179}\text{Hf}_s < 0$) cannot account for the resolved r-process Hf excess in CAI_NV_3 and potentially CAI_PS_4 ($\varepsilon^{177,179}\text{Hf}_s > 0$). CAI_PS_4, although overlapping within the analytical uncertainty with CAI_NV_3, does not show clearly resolved Hf isotope variations ($\varepsilon^{177}\text{Hf}_s = 0.10 \pm 0.29$, $\varepsilon^{179}\text{Hf}_s = 0.27 \pm 0.70$), and may have a terrestrial Hf isotope composition. For the resolved Hf isotope variation of CAI_NV_3, a simple two-component mixing model (terrestrial + r-deficit Hf) is insufficient. The isotopic composition of this CAI requires a third component, having an excess of r-process Hf, and this hints at the existence of an additional isolated reservoir (in time or space) from which this less common CAI formed.

3.5. Nucleosynthesis of Zirconium Isotopes

The existence of an early solar system reservoir with uniformly positive ε^{96}Zr and ε^{50}Ti, and the overall correlation of ^{96}Zr and ^{50}Ti variations in CAIs (Schönbächler et al. 2011; Leya et al. 2009; Harper et al. 1991) indicates a possible connection between ^{96}Zr and ^{50}Ti nucleosynthesis and thus supports a common astrophysical site for the co-production of ^{96}Zr and ^{50}Ti. This is potentially a supernova environment, as previously suggested by Harper et al. (1991). The original ^{96}Zr/^{50}Ti production ratio may have been altered (e.g., by mixing with materials from other sources) after the time of nuclide formation in the parent star(s) until their incorporation into CAIs. Assuming that this alteration is most probably a dilution with average solar system material, it is possible to use the ^{96}Zr–^{50}Ti co-variation to obtain constraints on the production sites of ^{96}Zr that contributed material to CAIs. This is discussed in the following sections. Once such a site is identified, we explore whether this site can also explain the Hf isotope variations in CAIs and the lack thereof in bulk carbonaceous chondrites. The plausibility of AGB stars, SNeIa, or SNeII as potential production sites, as well as the potential production mechanisms of ^{96}Zr, are discussed.

3.5.1. AGB Stars

Nucleosynthetic models show that low mass AGB stars are largely responsible for the synthesis of the s-process component of Zr (Bisterzo et al. 2011; Travaglio et al. 2004). However, only small amounts of ^{96}Zr are synthesized in these AGB stars relative to ^{90,91,92,94}Zr. This suggests that the Zr isotope composition produced in AGB stars exhibit—on average—strong ^{96}Zr depletions relative to average solar system material. This is supported by the Zr isotope composition of mainstream SiC grains, which are thought to originate from AGB stars (Nicolussi et al. 1997; Zinner 2007). They generally exhibit large depletions in ^{96}Zr (Nicolussi et al. 1997; Davis et al. 1999a). At the same time, mainstream SiC grains are characterized by ^{50}Ti excesses (Hoppe et al. 1994). Nucleosynthetic models also predict enrichments in ^{50}Ti for AGB stars (Gallino et al. 1990; Cristallo et al. 2011). Therefore, AGB stars produce materials with ^{96}Zr depletions and ^{50}Ti excesses, which is unlike the correlated ^{50}Ti–^{96}Zr excesses in CAIs. Therefore, the AGB stars are unlikely sources for the correlated ^{96}Zr–^{50}Ti excesses in CAIs.

3.5.2. Type Ia Supernovae

SNeIa are thermonuclear explosions of white dwarf (WD) stars in a binary system. They involve the low entropy expansion of neutron-rich matter, where neutron-rich isotopes of the Fe-group form (Meyer 1994). Under such conditions, the density is high enough for electron-capture reactions to occur, driving the matter neutron-rich, and toward a weak nuclear statistical equilibrium (W-NSE). As the temperature drops, a reaction freeze-out occurs, leaving behind a distribution of mass fractions dominated by the neutron-rich Fe-group isotopes (Hartmann et al. 1985; Meyer et al. 1996). In such an environment, large amounts of ^{50}Ti, ^{48}Ca, and other neutron-rich isotopes are produced and such nucleosynthesis can explain the roughly correlated excesses and deficits of ^{48}Ca, ^{50}Ti, and ^{54}Cr

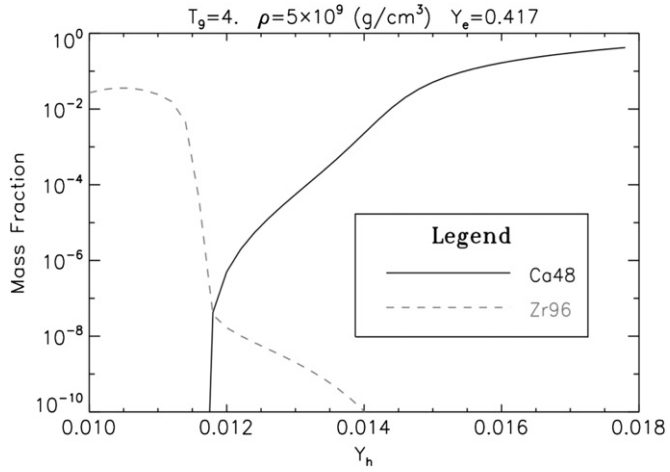

Figure 5. ^{96}Zr and ^{48}Ca yields for SNeIa. Mass fractions of ^{48}Ca and ^{96}Zr are calculated for different entropy conditions within an SNIa, at a constant temperature (T), electron fraction (Y_e) and density (ρ), as defined in the legend (Yu and Meyer 2011). The entropy is expressed as the heavy element ($Z > 6$) fraction, Y_h. In the low entropy case (high Y_h), ^{48}Ca production is more favorable because most nucleons prefer the most stable nuclei, for a given Y_e. In the high entropy case (low Y_h), many light particles (p, n, α) are available to produce heavier nuclei than ^{48}Ca. (Figure reproduced with permission from T. Yu.)

reported for FUN CAIs (Meyer et al. 1996). More recently, this environment was also considered as the source of ^{50}Ti and ^{48}Ca excesses in normal CAIs (e.g., Chen et al. 2011). However, the co-production of ^{48}Ca with ^{96}Zr is unlikely because they require different entropy conditions (Figure 5). In the low entropy (high values of heavy nuclei abundance, Y_h) environment of the SNIa, in which the Fe-group nuclei ($Y_h > 0.012$) are synthesized, the production of ^{96}Zr is not expected. It is therefore unlikely that the correlated ^{96}Zr and ^{50}Ti excesses in normal CAIs are synthesized together in the low entropy environment of an SNIa.

Another possibility to potentially co-synthesize ^{96}Zr and ^{50}Ti in SNeIa was recently presented by Travaglio et al. (2011), who proposed that small amounts of ^{96}Zr are associated with SNeIa, accompanying p-process nuclide production. The authors show that the p-process occurs in such sites only if the progenitor WD is initially enriched in s-process nuclides, which act as the seed nuclei for the p-process. The initial s-process enrichment of the WD is established in its earlier TP-AGB phase and can be modeled using the stellar yields of Gallino et al. (1998) and Bisterzo et al. (2010; 2011). During the accretion of matter from its companion main sequence or evolved star, the WD undergoes further thermal pulses, leading to more s-process nucleosynthesis. Soon after (~0.6 s) the ignition of the SNIa, ^{22}Ne burning proceeds in the outer layers of the WD, producing increased amounts of ^{96}Zr by the neutron-capture reaction ^{95}Zr(n,γ)^{96}Zr. Closer to the inner layers of the WD and when the temperature exceeds 2×10^9 K, ^{12}C nuclei become more abundant and ^{12}C burning dominates. Hence, the production of ^{96}Zr ceases. During this phase p-nuclei are produced through photo-disintegration reactions (e.g., ^{91}Nb(γ, p)^{90}Zr and ^{91}Zr(γ, n)^{90}Zr), replenishing the ^{90}Zr that was initially lost through neutron-capture.

In summary, the explosive ^{22}Ne-burning phase produces large quantities of ^{96}Zr in an SNIa augmenting relics of ^{96}Zr from the initial s-process phase. The resulting ε^{50}Ti/ε^{96}Zr of –0.5 (Travaglio et al. 2011) is lower than our CAI value (ε^{50}Ti/ε^{96}Zr = 5; Ti data normalized to ^{49}Ti/^{47}Ti, Leya et al. 2009). The isotopic signatures sampled by CAIs may represent mixtures between SNe material with the average solar system material (CI chondrites) that possess low ε^{50}Ti/ε^{96}Zr of ~1 (Leya et al. 2008, Schönbächler et al. 2003). Such mixing (SNIa–CI) will not be able to reach the high CAI ε^{50}Ti/ε^{96}Zr value of 5. Moreover, the seed nuclei for the WD were chosen arbitrarily, which can artificially enhance the s-production of ^{96}Zr. Thus, the predicted ε^{50}Ti/ε^{96}Zr value (–0.5) is an upper limit. Since the model predictions do not match the observations, the proposed process is unlikely to be the source of the ^{96}Zr isotope enrichments in CAIs.

In summary, the SNeIa environments are improbable sites for the production of the ^{96}Zr variations observed in CAIs, because nucleosynthetic models describing the isotopic yields within this environment fail to predict the ^{96}Zr variations that are observed in combination with other isotopic effects (e.g., ^{50}Ti, ^{48}Ca) in CAIs.

3.5.3. Type II Supernovae

The SNII environment was proposed as the likely site of r-process nucleosynthesis (e.g., Cowan et al. 1991; Meyer 1994; Argast et al. 2004). Within this environment, ^{50}Ti, ^{96}Zr, and r-process Hf isotopes can be produced in variable proportions in the different mass shells (Rauscher et al. 2002). This can potentially lead to co-variations in r-process isotopes in solar system materials.

3.5.3.1. The Decoupling of Zr and Hf Isotopes: Implications

In order to identify collateral r-process Hf isotope variations and to simplify the interpretation, the Hf isotope data previously reported by Sprung et al. (2010) were re-normalized relative to the two dominantly s-process isotopes (^{178}Hf/^{180}Hf; Table 3, Figure 4). The re-normalized data show that the s- and r-process isotopes of Hf in carbonaceous chondrites are homogeneously distributed and resolvable anomalies are not detected, consistent with the results using the ^{179}Hf/^{177}Hf renormalization scheme (Sprung et al. 2010). This stands in contrast to the well-resolved positive ε^{96}Zr in bulk carbonaceous chondrites (Table 3). In line with our findings, isotopic homogeneity at the bulk rock scale is reported for other main r-process isotopes such as Sm, Nd, and W isotopes (Andreasen & Sharma 2007; Carlson et al. 2007; Burkhardt et al. 2011), while isotopic anomalies are reported in lighter elements (e.g. for Mo, Burkhardt et al. 2011). Based on this data alone, however, it is impossible to distinguish whether the difference is due to a decoupling of the nucleosynthetic processes that produced Zr and Hf isotopes or whether it reflects correlated Hf isotope anomalies that are below the detection limits of our current analytical capabilities.

Interestingly, the CAIs with the exception of CAI_NV_3 and CAI_PS_4 exhibit ε^{177}Hf and ε^{179}Hf values that imply a depletion of r-process isotopes. The CAIs with this depletion also possess the strongest ε^{96}Zr excesses (Figure 4) and this indicates a separate production site for Hf and Zr r-process isotopes. This finding further corroborates previous studies that presented evidence for a decoupling of the sources of the high mass ($A > 130$) or main r-process component and low mass ($A < 130$) elements (Wasserburg et al. 1996; Qian & Wasserburg 2007; Wasserburg & Qian 2009; Ott & Kratz 2008; Andreasen & Sharma 2007).

3.5.3.2. Production Mechanism of ^{96}Zr (And Other Light Neutron-capture Elements) within Type II Supernova: CPR or Weak r-process?

While the nucleosynthesis of the main r-process component is relatively well understood, considerable disagreement exists

about the nature and extent of the low mass component ($A < 130$, $Z \leqslant 56$; e.g., Argast et al. 2004; Qian & Wasserburg 2007). Overall, Woosley et al. (1994) identified two different epochs in the SNII explosion phase, where different elements can be synthesized. In the *initial* neutrino-heated ejecta, light ($Z < 56$) r-process elements are produced. The final abundances of these light elements are very sensitive to the electron fraction and are, therefore, different for every supernova event. The *later* neutrino-driven wind further out generates the heavier elements and is thought to take place under similar physical conditions for each supernova, giving rise to a general abundance pattern in SNeII.

Kratz and co-workers (Kratz et al. 2008; Farouqi 2005; Farouqi et al. 2010) explored nucleosynthetic yields in the neutrino-driven (high entropy) wind. The astrophysical conditions were characterized using three interrelated parameters: electron fraction (Y_e), expansion velocity (v_e), and entropy ($S \sim T^3/\rho$; T—temperature, ρ—density of matter). In such an environment, nucleosynthesis can be sub-divided into (1) CPRs and (2) neutron-captures. Case (1) involves neutron-induced ((n, γ), (n, p), (n, α)), proton-induced ((p, γ), (p, n), (p, α)), and α-particle-induced ((α, γ), (α, n), (α, p)) reactions and their inverses, in addition to beta-decay. Case (2) is limited to neutron-induced reactions and beta-decay. The activation, or dominance, of these two sets of reactions depends on the presence of free α-particles or neutrons. At high densities (low entropies), the triple-α reaction ($3\alpha \rightarrow {}^{12}$C) and $\alpha\alpha$n ($\alpha\alpha$n$\rightarrow {}^{9}$Be(α, n)^{12}C) reactions are active and lock up α-particles and neutrons into heavier nuclei toward the Fe group. In such an environment, no free neutrons are available for neutron-captures and the CPRs dominate, capable of synthesizing elements up to Pd ($Z = 46$, $A = 130$). However, in the outer, lower density (high entropy) mass shells, the triple-α and $\alpha\alpha$n reactions are not as effective, leaving α-particles and neutrons available for other reactions. Neutron-capture can therefore take place and constitutes a weak r-process at relatively moderate neutron-to-seed ratios (n/seed $\sim$ 20–50) or the main r-process (n/seed ratio $>$50–100; Kratz et al. 2008). Collectively, the CPRs and neutron-captures will synthesize elements (with distinct contributions) in the different mass (entropy) shells of the neutrino-driven wind of an SNII.

The isotope ^{96}Zr is considered a weak r-process isotope and therefore is expected to form in an environment with relatively moderate neutron-to-seed ratios that are intermediate of the s-process (n/seed $\sim$ 1–2) and the main r-process. Various studies (Farouqi et al. 2010; Kratz et al. 2008; O. Hallmann & K.-L. Kratz 2013, private communication) showed that for a range of electron fractions (e.g., $0.4 \leqslant Y_e \leqslant 0.46$) all five Zr isotopes are produced. Regardless of the Y_e value, the CPRs dominate ($\sim$75%) the ^{96}Zr production, while the weak r-process contributes $\sim$20% of the total SN yield. The remaining 5% is attributed to the main r-process. It is important to note that CPRs do not produce Hf isotopes. These are either produced via the main r-process in the outer shells, or a different mass range (8–11 $M_\odot$) of SNeII altogether (e.g., Farouqi et al. 2010; Qian et al. 1998; Wasserburg & Qian 2000b). Thus, it is evident that the CPR component of an SNII is capable of producing enrichments in ^{96}Zr with no net effect on Hf isotopes, which can explain the ^{96}Zr excesses in the CAIs.

Farouqi et al. (2010) adopt a site-independent approach to the CPR model, whereas Wasserburg & Qian (2009) propose CPRs to take place in low mass (8–11 $M_\odot$) and normal mass (12–25 $M_\odot$) SNeII. Based on the latter work, CPRs produce ^{96}Zr in low mass and normal mass SNeII (Table 5). The production of r-process Hf isotopes, however, is limited to the main r-process in low mass SNeII. Hence, the observation of ^{96}Zr excesses alongside with deficits in r-process Hf isotopes suggests that the bulk of the CAIs sampled material from a normal mass SNII.

Table 5
Different CPR and r-process Contributions to Zr and Hf from SNeII

	Low mass SN		Normal mass SN	
	CPR	r-process	CPR	r-process
Zr	Yes	No	Yes	Yes
Hf	No	Yes	No	No

Note. The r-process refers to both the weak- and main- r-process contributions.

Taking this conclusion one step further by considering the ^{96}Zr–^{50}Ti co-variations of CAIs, CPRs do not produce enough ^{50}Ti (relative to ^{96}Zr) to explain this CAI data. However, significant ^{50}Ti can also be synthesized during the pre-supernova phase (Rauscher et al. 2002) and can compensate for the low yield during CPRs. Hence, although ^{96}Zr and ^{50}Ti are primarily not produced in the same site during the evolution of an SNII, later mixing of different zones (e.g., during the supernova explosion) can satisfy the CAI data. Interestingly, Qin et al. (2011) and Steele et al. (2012) also favor a normal mass ($\sim$15 $M_\odot$) SNII for the production of ^{50}Ti, ^{54}Cr, and ^{58}Ni isotope anomalies, in bulk solar system materials. Both studies succeeded to co-produce these three isotopes in an SNII followed by mixing of various burning shells (O/Ne and O/C for Cr; Si/S for Ti) in the star, prior to the supernova explosion.

Tentatively, we compared the Zr isotope ratios of CAIs to stellar yields during the pre- and post-supernova phases (Rauscher et al. 2002) using the method of Steele et al. (2012). The results indicate that the boundary region between the O/C and He/C burning zones may be able to produce the Zr isotope pattern captured by CAIs. However, this result should be regarded with caution because the stellar yield calculations from Rauscher et al. (2002) do not incorporate mechanisms for r-process synthesis or the full set of CPRs used by Farouqi (2005) and Farouqi et al. (2010).

3.5.3.3. Evidence from Presolar Grains

A rare subset ($\sim$1%) of presolar grains—Type X grains—bears testimony to supernovae nucleosynthesis. These grains exhibit large excesses in ^{96}Zr relative to ^{90,91,92,94}Zr compared to average solar system material (Pellin et al. 2006; Davis et al. 1999b). Their isotopic signatures for Zr (and also Mo and Ru) can be explained by neutron burst models for exploding stars (Meyer et al. 2000; Howard et al. 1992). Alternatively, Farouqi et al. (2010) and Hallmann et al. (2013) favor CPRs within the neutrino-driven wind of an SNII as the origin of ^{96}Zr enrichments in Type X grains because in contrast to the neutron burst model, the CPR model does not rely on an arbitrarily chosen initial seed distribution. It is therefore conceivable that the ^{96}Zr excesses observed in both CAIs and Type X grains are due to charged-particle nucleosynthesis within the neutrino-driven wind of an SNII.

However, CAIs show correlated ^{96}Zr–^{50}Ti excesses, whereas Type X grains do not exhibit ^{50}Ti variations (Amari et al. 1992, Hoppe & Besmehn 2002), but enrichments in ^{49}Ti (from the decay of ^{49}V; Hoppe & Besmehn 2002). A main difference

between CAIs and X grains is that X grains are thought to have condensed in a supernova environment, whereas CAIs formed later within our solar system and represent an amalgamation of many different presolar phases, which may include X grains. This raises the question of how much Type X grains CAIs could have sampled despite the different isotopic systematics. Taking the Ti concentration of CAIs and Type X grains as ~10,000 ppm (Mason & Taylor 1982) and 20–360 ppm (Amari et al. 1992), respectively, and Ti isotope compositions from Leya et al. (2009) and Amari et al. (1992), mass balance calculations reveal that CAIs can only contain an excess in Type X grains (compared to average solar system) that is $< 0.01\%$ in order to ensure that CAIs maintain a terrestrial ^{49}Ti abundance (Leya et al. 2009). Thus, CAIs did not collect significant excesses of Type X grains compared to average solar system material.

Moreover, for X grains produced by a neutron burst, the total amount of ^{96}Zr produced is small when compared to the integrated yield of all layers within the star. Therefore, X grains most likely represent a snapshot of supernova nucleosynthesis. Similarly, CPR produced material condensed in Type X grains would sample a limited amount of material. Since CAIs are a mixture of many presolar phases, the CAI-X grain contrast in ^{96}Zr–^{50}Ti coupling could reflect the more comprehensive collection of different supernova materials by CAIs.

4. CONCLUSIONS

We present new Zr and Hf isotope data for CAIs including high-precision Zr isotope compositions for carbonaceous chondrites and a terrestrial sample that were previously analyzed for Hf isotopes. The Zr data shows clearly resolved excesses in the neutron-rich, stable isotope, ^{96}Zr, while the new Hf data for all but two CAIs reveal depletions in r-process isotopes. These mass-independent shifts cannot be explained by galactic/cosmic ray spallation or the nuclear field shift and are very likely of nucleosynthetic origin. Our Zr isotope data obtained for the CM2 meteorite Murchison demonstrate that a hotplate digestion only achieves an incomplete digestion of refractory presolar grains, which leads to an artificial enrichment in ^{96}Zr/^{90}Zr. These effects can be negated using microwave or Parr bomb digestion procedures. The majority (75%) of CAIs are characterized by homogeneous ε^{96}Zr of an average 1.9 ± 0.1, $\varepsilon^{50}\mathrm{Ti} = 9.0 \pm 1.1$ (Leya et al. 2009), and $\varepsilon^{177}\mathrm{Hf}_s$ and $\varepsilon^{179}\mathrm{Hf}_s$ with averages of -0.10 ± 0.02 and -0.25 ± 0.02, respectively, relative to the terrestrial standard, while a subset of the CAIs show smaller excesses in ^{96}Zr and ^{50}Ti coupled with potential r-process enrichments in Hf. This indicates that (1) the source region of most CAIs was uniformly enriched in the neutron-rich ^{96}Zr, ^{50}Ti, and r-process deficient Hf, distinct from the source region of other planetary bodies, and (2) the likely co-production of ^{96}Zr and ^{50}Ti by the same source without significant production of Hf. The less extreme signature of the remaining 25% CAIs potentially reflects a dilution with average solar system material. However, the resolved excess in r-process Hf in one of these CAIs rather points toward the presence of a third nucleosynthetic reservoir. This could be achieved by various degrees of thermal processing of a previously homogeneous solar nebula, that left different mixtures of presolar phases behind. The evaluation of co-synthesis of ^{96}Zr, ^{50}Ti, and Hf isotopes in SNeIa, SNeII, and AGB stars reveals that different evolutionary phases of the SNII best explain the data. This source is different to the SNIa source suggested for the isotopic variations in neutron-rich isotopes of the Fe group elements in FUN inclusions (Meyer et al. 1996; Meyer 1997).

Different production sites for light ($Z \leqslant 56$) and heavy ($Z > 56$) neutron-rich nuclei explain the observed decoupling of the Zr and Hf isotope data. The synthesis of ^{96}Zr is expected to take place in low (8–11 $M_\odot$) and normal (12–25 $M_\odot$) mass SNeII, mainly by CPRs in the neutrino-driven wind close to the proto-neutron star during collapse. A small neutron-capture (weak r-process) contribution from normal mass SNeII, and some unknown contribution form the pre-supernovae phase is also expected. Abundant Hf, however, is synthesized through the r-process in SNeII with low mass progenitors only. The Zr and Hf isotope signatures of CAIs therefore indicate that CAIs sampled an excess of neutron-rich matter ($Z \leqslant 56$) from a normal mass SNII. This material could have originated from a nearby supernova that triggered the formation of the solar system (Cameron & Truran 1977), although our study does not provide any time constraints.

W.A. acknowledges support from the Science and Technology Facilities Council (UK) for the PhD studentship. P.S. acknowledges funding from the Deutsche Forschungsgemeinschaft via DFG grant SP 1385/1–1. We thank C. Davies and K. Theis for technical assistance in the labs, K. Bermingham for the laser-fusion CAI samples, and O. Hallmann and K.-L. Kratz for valuable comments on their CPR network and for providing us with their unpublished data for Zr. We also thank the reviewer, P. Hoppe, for his valuable comments to improve this manuscript. We acknowledge T. Yu for giving us permission to reprint Figure 5.

REFERENCES

Akram, W. 2013, PhD thesis, The Univ. of Manchester
Alpher, R. A., Bethe, H., & Gamow, B. 1948, PhRv, 73, 803
Amari, S., Hoppe, P., Zinner, E., & Lewis, R. S. 1992, ApJ, 394, L43
Amari, S., Hoppe, P., Zinner, E., & Lewis, R. S. 1995, Metic, 30, 679
Anders, E., & Zinner, E. 1993, Metic, 28, 490
Andreasen, R., & Sharma, M. 2006, Sci, 314, 806
Andreasen, R., & Sharma, M. 2007, ApJ, 665, 874
Angeli, I. 2004, ADNDT, 87, 185
Argast, D., Samland, M., Thielemann, F.–K., & Qian, Y.–Z. 2004, A&A, 416, 997
Arlandini, C., Käppeler, F., Wisshak, K., et al. 1999, ApJ, 525, 886
Bigeleisen, J. 1996, J. Am. Chem. Soc., 118, 3676
Birck, J.–L. 2004, Rev. Min. Geochem., 55, 25
Bisterzo, S., Gallino, R., Straniero, O., Cristallo, S., & Käppeler, F. 2010, MNRAS, 404, 1529
Bisterzo, S., Gallino, R., Straniero, O., Cristallo, S., & Käppeler, F. 2011, MNRAS, 418, 284
Brandon, A. D., Humayun, M., Puchtel, I. S., Leya, I., & Zolensky, M. 2005, Sci, 309, 1233
Brennecka, G. A., Borg, L. E., & Wadwha, M. 2011, Lunar Planet Sci. Conf. XXXXII 43, Abstract No. 2006
Burbidge, E. M., Burbidge, G. R., Fowler, W. A., & Hoyle, F. 1957, RVMP, 29, 547
Burkhardt, C., Kleine, T., Oberli, F., et al. 2011, E&PSL, 312, 390
Burris, D., Pilachowski, C. A., Armandroff, T. E., et al. 2000, ApJ, 544, 302
Cameron, A. G. W. 1957, PASP, 169, 201
Cameron, A. G. W. 1973, SSRv, 15, 121
Cameron, A. G. W., & Truran, J. W. 1977, Icar, 30, 447
Carlson, R. W., Boyet, M., & Horan, M. 2007, Sci, 316, 1175
Chen, H.–W., Lee, T., Lee, D.–C., Shen, J. J.–S., & Chen, J.–C. 2011, ApJL, 743, L23
Cowan, J. J., Burris, D. L., Sneden, C., McWilliam, A., & Preston, G. W. 1995, ApJ, 439, L51
Cowan, J. J., Thielemann, F.–K., & Truran, J. W. 1991, PhR, 208, 267
Cristallo, S., Piersanti, L., Straniero, O., et al. 2011, ApJ, 197, 17
Davis, A. M. 2004, in The r-Process: the Astrophysical Origin of the Heavy elements and Related Rare Isotope Accelerator Physics, ed. Y.-Z. Qian, E. Rehn, H. Schatz, & F.-K. Thielemann World Scientific), 120

Davis, A. M., Nicolussi, G. K., Pellin, M. J., Lewis, R. S., & Clayton, R. N. 1999a, in Nuclei in the Cosmos V, ed. N. Prantzos & S. Harissopulos (Paris: JSF Editions), 563
Davis, A. M., Pellin, M. J., Lewis, R. S., Amari, S., & Clayton, R. N. 1999b, M&PS, 34, A30
Farouqi, K. 2005, PhD thesis, Univ. of Mainz
Farouqi, K., Kratz, K.-L., Pfeiffer, B., et al. 2010, ApJ, 712, 1359
Fujii, T., Moriyama, H., Hirata, T., & Nishizawa, K. 2001, B. Chem. Soc. Jpn., 74, 1031
Fujii, T., Moynier, F., & Albarede, F. 2006, E&PSL, 247, 1
Gallino, R., Busso, M., Picchio, G., & Raiteri, C. M. 1990, Natur, 348, 298
Gallino, R., Busso, M., Picchio, G., Raiteri, C. M., & Renzini, A. 1988, ApJ, 334, 45
Gallino, R., Travaglio, C., Busso, M., et al. 1998, ApJ, 497, 388
Gamow, G. 1946, PhRv, 70, 572
Hallmann, O., Farouqi, K., Kratz, K.-L., & Ott, U. 2013, M&PS, 5082
Harper, C. L., Wiesmann, H., Nyquist, L. E., et al. 1991, Lunar Planet Sci. Conf. XXX, Abstract No. 22, 517
Hartmann, D., Woosley, S. E., & El Eid, M. F. 1985, ApJ, 297, 837
Honda, S., Aoki, W., Kajino, T., et al. 2004, ApJ, 607, 474
Hoppe, P., Amari, S., Zinner, E., Ireland, T., & Lewis, R. S. 1994, ApJ, 430, 870
Hoppe, P., & Besmehn, A. 2002, ApJ, 576, L69
Howard, M. W., Meyer, B. S., & Clayton, D. D. 1992, Metic, 27, 404
Huss, G. R. 1997, in AIP Conf. Proc. 402, Astrophysical Implications of the Laboratory Study of Presolar Materials, ed. T. J. Bernatowicz & E. K. Zinner (Melville, NY: AIP), 721
Käppeler, F., Beer, H., & Wisshak, K. 1989, RPPh, 52, 945
Kratz, K.-L., Farouqi, K., Mashonkina, L. I., & Pfeiffer, B. 2008, NewAR, 52, 390
Lauretta, D. S., & McSween, H. Y. 2006, Meteorites and the Early Solar System II (Tucson, AZ: Univ. Arizona Press)
Leya, I., Schönbächler, M., Krähenbühl, U., & Halliday, A. N. 2009, ApJ, 702, 1118
Leya, I., Schönbächler, M., Wiechert, U., Krähenbühl, U., & Halliday, A. N. 2008, E&PSL, 266, 233
Leya, I., Wieler, R., & Halliday, A. N. 2003, GeCoA, 67, 529
Lodders, K. 2003, ApJ, 591, 1220
Lodders, K., Palme, H., & Gail, H.-P. 2009, A&A, 4, 34
Lugaro, M., Davis, A. M., Gallino, R., et al. 2003, ApJ, 593, 486
Mason, B., & Taylor, S. R. 1982, SmCES, 25, 1
Merchel, S., Ott, U., Herrmann, S., et al. 2003, GeCoA, 67, 4949
Meyer, B. 1994, ARA&A, 32, 153
Meyer, B. 1997, M&PS, 32, A92
Meyer, B., Clayton, D. D., & The, L. S. 2000, ApJL, 540, 49
Meyer, B., The, L.-S., & El Eid, M. F. 1996, Lunar Planet Sci. Conf XXVII Abstract No. 875, 27
Minster, J. F., & Allègre, C. J. 1982, GeCoA, 46, 565
Minster, J. F., & Ricard, L. P. 1981, IJMSI, 37, 259
Nicolussi, G. K., Davis, A. M., Pellin, M. J., et al. 1997, Sci, 277, 1281
Nicolussi, G. K., Pellin, M. J., Lewis, R. S., et al. 1998, ApJ, 504, 492
Ott, U., & Kratz, K.-L. 2008, NewAR, 52, 396
Pack, A., Kremer, K., Albrecht, N., Simon, K., & Kronz, A. 2010, Geochem. Trans., 11, 1
Patzer, A., Pack, A., & Gerdes, A. 2010, M&PS, 45, 1136
Pellin, M. J., Savina, M. R., Calaway, W. F., et al. 2006, Lunar Planet Sci. Conf. XXXVII Abstract, 2041
Preiswerk, L. 2011, BSc thesis, ETH Zurich
Qian, Y.-Z., Vogel, P., & Wasserburg, G. J. 1998, ApJ, 506, 868
Qian, Y.-Z., & Wasserburg, G. J. 2007, PhR, 442, 237
Qin, L., Nittler, L. R., Alexander, C. M. O'D., et al. 2011, GeCoA, 75, 629
Quitté, G., Halliday, A. N., Meyer, B. S., et al. 2007, ApJ, 655, 678
Raiteri, C. M., Gallino, R., Busso, M., Neuberger, D., & Käppeler, F. 1993, ApJ, 419, 207
Rauscher, T., Heger, A., Hoffman, R. D., & Woosley, S. E. 2002, ApJ, 576, 323
Schönbächler, M., Akram, W., Williams, N. H., & Leya, I. 2011, Formation of the First Solids in the Solar System, Abstract No. 9085
Schönbächler, M., Lee, D.-C., Rehkämper, M., et al. 2003, E&PSL, 216, 467
Schönbächler, M., Rehkämper, M., Lee, D.-C., & Halliday, A. N. 2004, Analyst., 129, 32
Schönbächler, M., Rehkämper, M., Fehr, M. A., et al. 2005, GeCoA, 69, 5133
Sneden, C., Cowan, J. J., Ivans, I. I., et al. 2000, ApJL, 533, L139
Sneden, C., Cowan, J. J., Lawler, J. E., et al. 2003, ApJ, 591, 936
Sneden, C., McWilliam, A., Preston, G. W., et al. 1996, ApJ, 467, 819
Sorlin, O., Gaudefroy, L., Kratz, K.-L., & Rauscher, T. 2003, C R Physique., 4, 451
Sprung, P., Kleine, T., & Scherer, E. E. 2013, EPSL, 380, 77
Sprung, P., Scherer, E. E., Upadhyay, D., Leya, I., & Mezger, K. 2010, E&PSL, 295, 1
Steele, R. C. J., Coath, C. D., Regelous, M., Russell, S., & Elliott, T. 2012, ApJ, 758, 59
Travaglio, C., Gallino, R., Arnone, R., et al. 2004, ApJ, 601, 864
Travaglio, C., Ropke, F. K., Gallino, R., & Hillebrandt, W. 2011, ApJ, 739, 93
Trinquier, A., Elliott, T., Ulfbeck, D., et al. 2009, Sci, 324, 374
Wasserburg, G. J., Busso, M., & Gallino, R. 1996, ApJL, 466, 109
Wasserburg, G. J., & Qian, Y.-Z. 2000a, ApJL, 538, L99
Wasserburg, G. J., & Qian, Y.-Z. 2000b, ApJL, 529, L21
Wasserburg, G. J., & Qian, Y.-Z. 2009, PASA, 26, 184
Wilson, S. A. 1998, Geological Survey Open-file Report (in press)
Woosley, S. E., Wilson, J. R., Mathews, G. J., Hoffman, R. D., & Meyer, B. 1994, ApJ, 433, 229
Yin, Q.-Y., Lee, C., –T., A., & Ott, U. 2006, ApJ, 647, 676
Yu, T., & Meyer, B. S. 2011, M&PSA, 74, 5453
Zhang, J., Dauphas, N., Davis, A. M., Leya, I., & Fedkin, A. 2012, NatGe, 5, 251
Zinner, E. 2007, in Meteorites, Comets, and Planets, ed. A. M. Davis (Oxford: Elsevier), 1